Supporting Information

Drescher et al. 10.1073/pnas.1300321110

SI Text

Influence of Biofilm Streamers on the Permeability of a Channel. We consider two elementary cases of biomass distribution to evaluate their effect on the permeability of a channel subjected to a pressure-driven flow. In one case, the biomass forms a thin film on the surface of the channel (Fig. S2*A*), whereas in the second case the biomass forms a single biofilm streamer in the center of the channel (Fig. S2*B*). For simplicity, we model the channel as a cylindrical pipe of radius ρ.

In the case of the wall-attached biofilm, the biofilm thickness is $\varepsilon\rho$, where $0 \le \varepsilon \ll 1$. For steady pressure-driven flow in a cylindrical channel, the classical Poiseuille formula relates the flow rate Q_0 to the total pressure drop across the whole channel per unit length $\Delta p_{\text{tot}}/L$, given by

$$Q_0 = \frac{\pi}{8}\frac{\rho^4 \Delta p_{\text{tot}}}{\eta L}, \qquad \text{[S1]}$$

where η is the dynamic viscosity of the fluid. When biofilm accumulates as a thin film on the walls of the channel, as indicated in Fig. S2*A*, the flow rate is obtained by using the new radius $\rho(1-\varepsilon)$. Therefore, for the identical pressure drop per unit length, the flow rate in the presence of a surface-attached biofilm Q_{film} satisfies

$$\frac{Q_{\text{film}}}{Q_0} = (1-\varepsilon)^4, \qquad \text{[S2]}$$

which reduces to $Q_{\text{film}}/Q_0 \approx 1 - 4\varepsilon$, with the assumption $\varepsilon \ll 1$.

In the case of a biofilm streamer positioned in the middle of the channel, we treat the streamer as a cylinder of radius R with a no-slip boundary. As shown in Movie S2, the biofilm streamer slowly moves along the flow, with a migration speed that is much lower than the flow speed. This finding justifies the assumption that the streamer provides a no-slip surface. The flow geometry thus reduces to the standard problem of a pressure-driven flow between two coaxial cylinders (1). Using cylindrical coordinates (radial coordinate r), the flow velocity along the direction of the cylinders is

$$u(r) = \frac{\rho^2 \Delta p_{\text{tot}}}{4\eta L}\left(1 - \left(\frac{r}{\rho}\right)^2 - \left[1 - \left(\frac{R}{\rho}\right)^2\right]\frac{\ln(r/\rho)}{\ln(R/\rho)}\right). \qquad \text{[S3]}$$

This velocity field can be integrated over the annular cross-section of the concentric cylinders to yield the flow rate in the presence of a streamer Q_{streamer}, which is given by

$$\frac{Q_{\text{streamer}}}{Q_0} = \frac{\left(\frac{R}{\rho}\right)^4 [1 - \ln(R/\rho)] + 1 + \ln(R/\rho) - 2\left(\frac{R}{\rho}\right)^2}{\ln(R/\rho)}. \qquad \text{[S4]}$$

To compare the flow rate reduction caused by the wall-attached biofilm with the flow-rate reduction caused by the streamer, we fix the streamer radius R such that the biomass in the streamer is equal to the biomass in the wall-attached biofilm. Due to cylindrical symmetry, $2\pi\rho^2\varepsilon = \pi R^2$, which can be rearranged to give $R = \rho(2\varepsilon)^{1/2}$. For small biofilms, $\varepsilon = 0.01 \ll 1$, we find

$$\frac{Q_{\text{film}}}{Q_0} = 1 - 4\varepsilon = 0.96, \qquad \text{[S5]}$$

$$\frac{Q_{\text{streamer}}}{Q_0} = 1 + \frac{2}{\ln \varepsilon} = 0.51. \qquad \text{[S6]}$$

Thus, a thin, wall-attached biofilm on the surface of the channel leads to a reduction in flow rate of a few percent, whereas the same biomass bound in a biofilm streamer along the centerline of the channel reduces the flow rate by ≈50%.

Growth of a Solid Biofilm Streamer. We consider a solid biofilm streamer with its axis oriented transverse to the flow direction, as in Fig. 3*A*. This orientation is motivated by Fig. S3, which shows that the streamers in our microfluidic system are partially transverse to the flow direction. We assume that the streamer radius R is much smaller than the channel diameter so that we can neglect the presence of the confinement and treat the streamer as a solid cylinder in an unbounded flow. We further assume that the streamer is very long so that the flow is essentially 2D and only varies in the plane that is orthogonal to the streamer axis.

For the low Reynolds numbers (Re) considered in our experiments, the flow around the streamer is laminar (Re = 0.1–2 for different flow rates). Cells that are carried by the flow can move across streamlines by the intrinsic diffusion of their cell body as well as their self-generated motility, which leads to an effective diffusion constant D. Diffusion across streamlines in the vicinity of the streamer can cause a cell to come in contact with the streamer, in which case we assume that there is a probability α that the streamer absorbs the cell. If the cell is absorbed by the streamer, the streamer expands its cross-sectional area by an area A. The growth rate of the cross-sectional area of the streamer is therefore given by

$$2\pi R\frac{\mathrm{d}R}{\mathrm{d}t} = \alpha I A, \qquad \text{[S7]}$$

where I is the number of cells per unit length of the streamer that come in contact with the streamer per unit time, and t is time. As cells are constantly absorbed by the streamer, the cell concentration c is expected to change close to the streamer, which, by Fick's law, causes a flux of cells $-D\nabla c$. This flux can be integrated over the cross-sectional area of the streamer S to obtain

$$I = -D\int \left[\frac{\partial c}{\partial r}\right]_{r=R} dS, \qquad \text{[S8]}$$

$$I = DC\ \text{Nu}, \qquad \text{[S9]}$$

where C is the cell concentration in the bulk far away from the streamer, and Nu is the mass transfer Nusselt number (also known as the Sherwood number). As we expect the growth rate of the streamer $\mathrm{d}R/\mathrm{d}t$ to be much smaller than the average flow speed V, the Nusselt number is governed by the time-independent advection–diffusion equation

$$D\nabla^2 c = (\mathbf{u}\cdot\nabla)c, \qquad \text{[S10]}$$

where $\mathbf{u}$ is the flow field around the streamer. The solution for $\mathbf{u}$ was obtained by Tomotika and Aoi (2). Using this solution for $\mathbf{u}$,

Friedlander (3) solved Eq. **S10** for c and showed theoretically that

$$\mathrm{Nu} \simeq \left(\frac{V\,R}{D(2-\log \mathrm{Re})}\right)^{1/3}. \quad \textbf{[S11]}$$

This result for Nu was confirmed experimentally for our values of the Reynolds number (4). Using $\mathrm{Re} \approx 1$, we obtain

$$I \simeq 0.8\, C\left(D^2 R V\right)^{1/3}. \quad \textbf{[S12]}$$

To solve Eq. **S7** for $R(t)$, we need to obtain an expression of Eq. **S12** in terms of R, which reduces to finding an expression for V in terms of R. Experimental studies on cylinders oriented transverse to the flow direction have shown that the drag force on the cylinder per unit length F obeys

$$F \approx 7\,\eta V \quad \textbf{[S13]}$$

for our values of the Reynolds number (5), which is consistent with theoretical results for F that are based on the solution for $\mathbf{u}$ (2). For an unbounded flow, the pressure difference Δp that drives the flow is equal to the pressure drop across the streamer. The streamer initiates across one turn of the model microfluidic channel and the pressure difference that drives the flow for such a section of the channel is $\Delta p \approx \Delta p_{\mathrm{tot}}/35$ (see Fig. 1*A* for an image of the channel, which has about 35 turns). As the pressure drop across the streamer occurs over a length scale R, the drag per unit length due to Δp is

$$F \approx E\,R\,\Delta p, \quad \textbf{[S14]}$$

where $E = \mathcal{O}(1) \sim 1$, analogous to the expression for the drag on a sphere. Combining our equations for F, we obtain

$$V \approx \frac{R\Delta p}{7\eta}. \quad \textbf{[S15]}$$

This expression for V is a peculiarity of 2D fluid mechanics, but can be substituted into Eq. **S12** to obtain $I \approx 0.4\, C(\Delta p\, D^2 R^2/\eta)^{1/3}$. This function for I can then be used to rearrange Eq. **S7**, yielding

$$\frac{\mathrm{d}R}{\mathrm{d}t} = BR^{-1/3}, \quad \textbf{[S16]}$$

where the constant is $B \approx 0.07\alpha CA(D^2\Delta p/\eta)^{1/3}$. This equation for $\mathrm{d}R/\mathrm{d}t$ can be solved easily to obtain

$$R(t) \approx \left(\frac{4}{3}Bt + \mathrm{const}\right)^{3/4}. \quad \textbf{[S17]}$$

Based on our expression for B and Eq. **S1** we can estimate the magnitude of B. Using our experimental parameters $C = 2 \times 10^{-4}$ cells/μm^3, $A = 2$ μm^3, $\rho = 75$ μm, $Q_0 = 10^{-9}$ m^3/min, $L = 2 \times 10^{-2}$ m, $D = 10^{-10}$ m^2/s, and $\Delta p \approx \Delta p_{\mathrm{tot}}/35$, we obtain $B \approx \alpha$ 20 μm$^{4/3}$/h. To understand the meaning of this value for B, we can complete the solution for $R(t)$ by fixing the integration constant in Eq. **S17** by setting $R(t = 0) = 10$ μm (motivated by Fig. S3). The dynamics of $R(t)$ for this condition are plotted in Fig. S5*A* for the upper bound $\alpha = 1$ (blue line) and $\alpha = 0.1$ (green line), which assumes that 100% or 10% of the cells that come in contact with the streamer are absorbed, respectively. To translate the dynamics of $R(t)$ into the dynamics of the flow rate $Q(t)$, we note that Fig. S3 shows that the streamer is oriented partly transverse and partly along the flow direction. We can therefore get a rough estimate of $Q(t)$ by using Eq. **S4**, which was derived for a streamer that is coaxial with a channel of circular cross-section. The resulting $Q(t)$ is plotted for $\alpha = 1$ and $\alpha = 0.1$ in Fig. S5*B*.

Fig. S5 shows that $R(t)$ and $Q(t)$ predicted by this model change too slowly to fully account for the rapid clogging transitions we observe experimentally. Although growth of streamers by the advection–diffusion process discussed in this section is likely to take place, the majority of the streamer growth is likely to be due to other mechanisms.

Growth of a Porous Biofilm Streamer. As in the discussion of the growth rate of a solid streamer above, we assume that the porous streamer is oriented transverse to the flow direction (motivated by Fig. S3) and that the streamer is very long so that the flow field only varies in the plane that is orthogonal to the streamer axis. The streamer is now assumed to be porous so that liquid and cells can flow through it, yet we still assume that the streamer radius is much smaller than the channel diameter so that we can neglect the effects of the channel walls.

If a cell that is caught by the streamer adds an area A to the cross-sectional area of the streamer, the rate of expansion of the streamer cross-section is given by

$$2\pi R\frac{\mathrm{d}R}{\mathrm{d}t} = \beta I\,A, \quad \textbf{[S18]}$$

analogous to Eq. **S7** for the solid streamer. However, now I is the number of cells per unit length of the streamer that flow through the streamer per unit time, and β is the fraction of these cells that get caught in the streamer. For simplicity, we calculate an upper bound on the streamer growth rate by assuming that the streamer is entirely transparent, i.e., cells flow through it at the same speed as if there was no streamer present. This means that there is a flux of cells $J = CV$ through the porous streamer, which results in

$$I = J\,2R. \quad \textbf{[S19]}$$

To solve the above differential equation for $R(t)$, we again use Eq. **S15** to obtain $I \approx 2C\Delta pR^2/\eta$, which we substitute into Eq. **S18** to obtain

$$\frac{\mathrm{d}R}{\mathrm{d}t} \approx \frac{\beta AC\Delta p}{7\pi\eta}R, \quad \textbf{[S20]}$$

which can be solved to give

$$R(t) \propto \exp\left(\frac{t}{\tau_{\mathrm{theory}}}\right), \quad \textbf{[S21]}$$

$$\tau_{\mathrm{theory}} \approx \frac{7\pi\eta}{\beta AC\Delta p}. \quad \textbf{[S22]}$$

We further note that Δp is proportional to the flow rate before the appearance of the streamer Q_0 (Eq. **S1**). The flow rate Q_0, in turn, is simply the average flow speed in the channel before the appearance of the streamer U multiplied by the cross-sectional area of the channel. The timescale of the exponential growth of the streamer can therefore be rewritten as

$$\tau_{\mathrm{theory}} \propto \frac{1}{CU}. \quad \textbf{[S23]}$$

The dependence $\tau_{\mathrm{theory}} \propto C^{-1}$ results from the assumption that the flux of cells that become caught in the streamer is simply proportional to the flux of cells that flow through the streamer,

i.e., $I = 2RVC$. Movie S2 illustrates that only a very small fraction of the cells actually gets caught. However, assuming that only 1% of the cells flowing through the streamer get caught (by setting $\beta = 0.01$) will not change the final functional dependence of τ_{theory} on C, except for a numerical prefactor. To obtain a relation that is closer to the experimental result $\tau \propto C^{-0.6}$, the number of cells that get caught must depend on the cell density. Such cell-density–dependent effects are plausible as 6–10% of the *Pseudomonas aeruginosa* genome is regulated by quorum sensing (6, 7), which may include genes responsible for adhesion to an existing biofilm.

We can estimate the magnitude of τ_{theory} using Eqs. **S22** and **S1**, and our experimental parameters $C = 2 \times 10^{-4}$ cells/μm^3, $A = 2$ μm^3, $\rho = 75$ μm, $Q_0 = 10^{-9}$ m^3/min, and $L = 2 \times 10^{-2}$ m. Bearing in mind that we derived an upper bound on the streamer growth rate in this model (see the comment above Eq. **S19**), which yields a lower bound on τ_{theory}, we can use these parameter values to obtain $\tau_{\text{theory}} \sim 0.02/\beta$ h. Although the exact value of β is unclear, Movie S2 illustrates that only a very small fraction of the cells gets caught in the streamer, and values of $\beta \sim 10^{-2}$ appear plausible, which yield values for τ_{theory} that are on the same order of magnitude as experimentally observed clogging timescales τ (Fig. 3).

Fig. S5*A* shows $R(t)$ for a porous streamer (Eq. **S21**) using $R(t = 0) = 10$ μm as an initial condition. Both models make strong simplifying assumptions, yet Fig. S5 shows that the model based on a porous streamer predicts a faster increase in R, which leads to a faster decrease of Q, compared with the model that describes streamer growth as an advection–diffusion process.

1. Bird RB, Stewart WE, Lightfoot EN (1960) *Transport Phenomena* (Wiley, New York).
2. Tomotika S, Aoi T (1950) The steady flow of viscous fluid past a sphere and circular cylinder at small Reynolds numbers. *Q J Mech Appl Math* 3:140–161.
3. Friedlander SK (1957) Mass and heat transfer to single spheres and cylinders at low Reynolds numbers. *AIChE J* 3:43–48.
4. Dobry R, Finn RK (1956) Mass transfer to a cylinder at low Reynolds numbers. *Ind Eng Chem* 48:1540–1543.
5. White CM (1946) The drag of cylinders in fluids at slow speeds. *Proc R Soc London, Ser A* 186:472–479.
6. Schuster M, Lostroh CP, Ogi T, Greenberg EP (2003) Identification, timing, and signal specificity of *Pseudomonas aeruginosa* quorum-controlled genes: A transcriptome analysis. *J Bacteriol* 185(7):2066–2079.
7. Wagner VE, Bushnell D, Passador L, Brooks AI, Iglewski BH (2003) Microarray analysis of *Pseudomonas aeruginosa* quorum-sensing regulons: Effects of growth phase and environment. *J Bacteriol* 185(7):2080–2095.

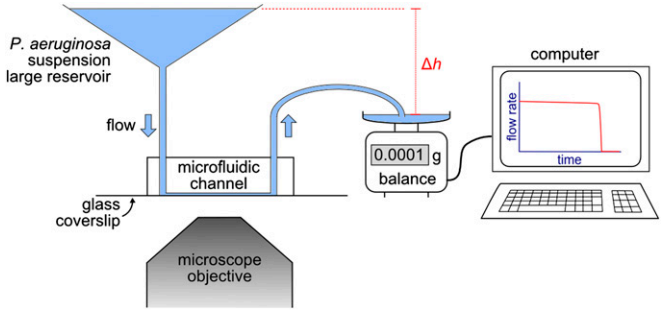

Fig. S1. Experimental setup. Midlogarithmic phase *P. aeruginosa* cells were loaded into a reservoir, with a large cross-sectional area at the air–water interface. The wide-bore tubing connects the microfluidic channel with the reservoir and the effluent collection dish, which is placed on an analytical balance. The height difference Δh between the reservoir suspension and the effluent collected on the analytical balance is proportional to the applied pressure. Data of the weight of the effluent as a function of time are converted on a computer to the flow rate as a function of time. The biofilm in the microfluidic channel, filter mesh, or stent, is imaged using a confocal or epifluorescence microscope.

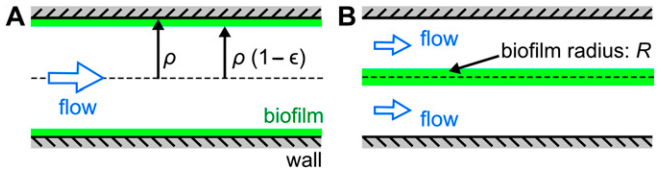

Fig. S2. Model geometries for calculating the influence of biofilm streamers on permeability. (*A*) Biofilm (green) forms as a thin film of thickness $\varepsilon\rho$ on the walls of a cylindrical channel with radius ρ. (*B*) Biofilm forms as a cylindrical streamer that is coaxial with the channel.

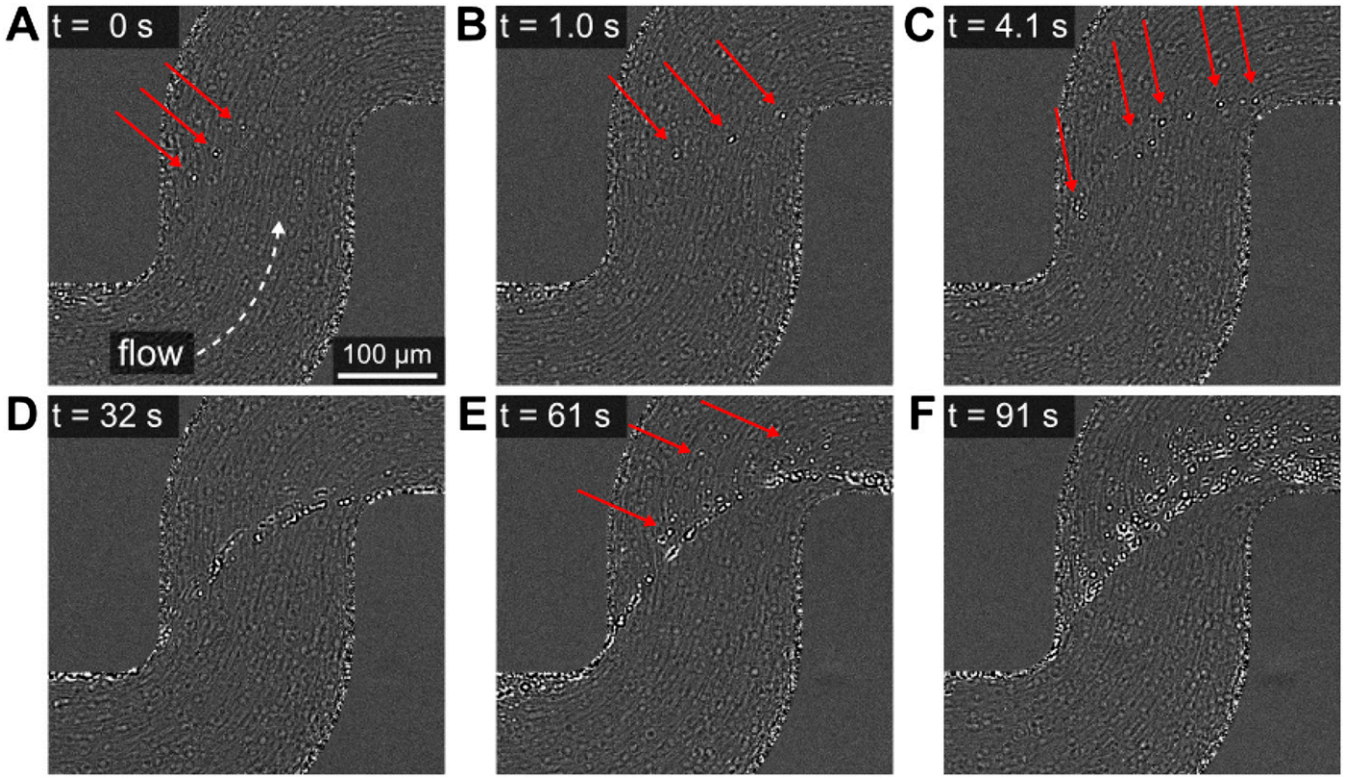

Fig. S3. Biofilm streamer initiation image sequence. Images were acquired at 30 frames per second using bright-field microscopy, and a background image was subtracted to visualize newly appearing structures such as streamers. The background image is made from the average of the 10 images taken 5 s before each image shown. Movie S2 shows the same process. (*A*) A thin streamer has formed, originating from the left corner. The streamer is not yet attached to the right corner. It appears to mostly consist of EPS, and only three cell/EPS clusters are visible. Red arrows point to these clusters. (*B*) The streamer has attached to the right corner, forming a biofilm bridge between the corners. The red arrows point to the same three clusters as in *A*, indicating that the streamer is now largely transverse to the flow direction in contrast with *A*. EPS: extracellular polymeric substances. (*C*) Additional cell/EPS clusters attach to the streamer, as indicated by the red arrows. At this stage, the streamer is flexible and vibrates in the flow. (*D*) The streamer has accumulated additional biomass and is less flexible. (*E*) Small secondary streamers are dragged out of the main streamer and appear to form a sieve-like network. Red arrows point to some of these secondary streamers. (*F*) The mesh of streamers that appeared in *E* has accumulated more biomass and new secondary streamers emerge.

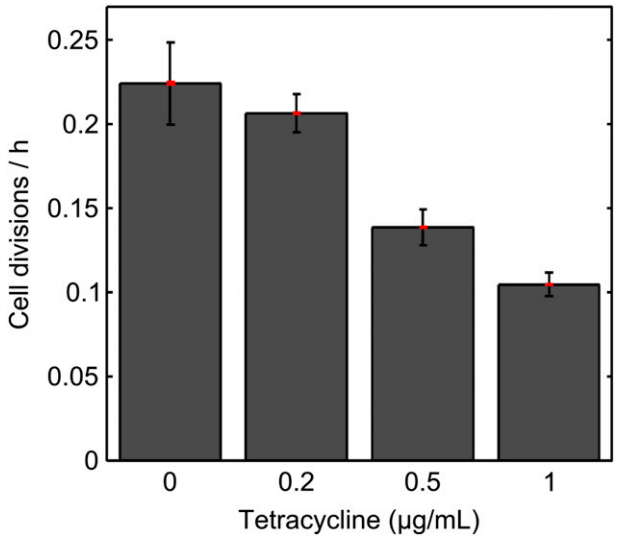

Fig. S4. Growth rate changes due to tetracycline. *P. aeruginosa* was grown at 22 °C in 96-well plates without shaking. By acquiring OD_{600} measurements every 20 min, growth curves were obtained from which we extracted the maximum growth rate for each well. Black error bars correspond to the SD of the growth rate observed in $n = 32$ different wells for each concentration of tetracycline, and red error bars correspond to the SEM. The minimum inhibitory concentration of tetracycline for *P. aeruginosa* is 32 µg/mL (1, 2).

1. Jayaraman P, Sakharkar MK, Lim CS, Tang TH, Sakharkar KR (2010) Activity and interactions of antibiotic and phytochemical combinations against *Pseudomonas aeruginosa in vitro*. *Int J Biol Sci* 6(6):556–568.
2. Toté K, et al. (2009) Inhibitory efficacy of various antibiotics on matrix and viable mass of *Staphylococcus aureus* and *Pseudomonas aeruginosa* biofilms. *Int J Antimicrob Agents* 33(6): 525–531.

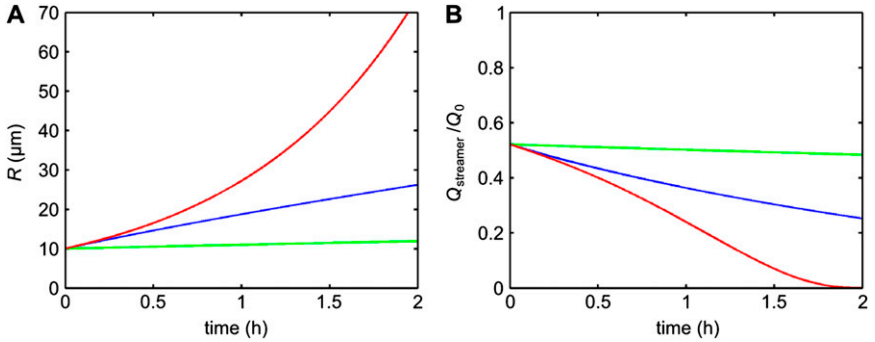

Fig. S5. Model results for dynamics of streamer growth and flow rate decrease. The model for streamer growth based on a porous streamer predicts the red lines in *A* and *B*, assuming $\tau_{theory} = 1$ h. The model based on an advection–diffusion process predicts the blue lines (for $\alpha = 1$) and the green lines (for $\alpha = 0.1$). Using the parameter $\alpha = 1$ leads to an upper bound on the streamer growth rate, as it implies that 100% of the cells that come in contact with the streamer are absorbed by it. Both models assume an initial condition of $R(t = 0) = 10$ μm. To estimate a conversion of the results for $R(t)$ into the flow rate $Q_{streamer}$, we used Eq. **S4**, which was derived for a streamer that is coaxial with a channel of circular cross-section, for which we assume a radius $\rho = 75$ μm. Both models make strong simplifying assumptions, yet the model based on a porous streamer yields results that more closely resemble the experimental dynamics.

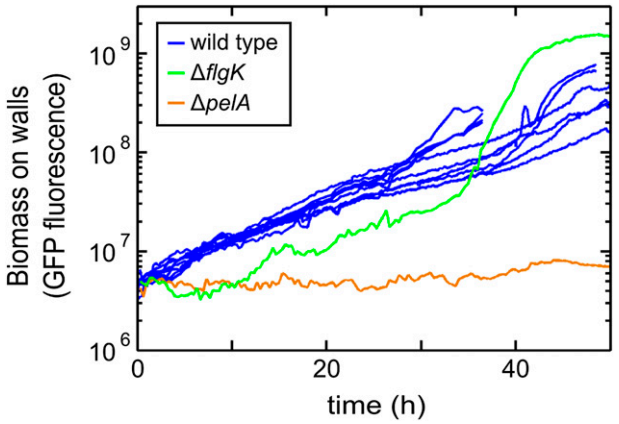

Fig. S6. Biomass increase for the Δ*flgK* and Δ*pelA* strains compared with the wild type. The flagella mutant strain displays a delay in biomass accumulation for the first ~10 h, but then increases in biomass with a doubling time comparable to the wild type. After ~35 h, the Δ*flgK* strain develops a streamer, which leads to a rapid increase in biomass. Over the same time the Δ*pelA* strain does not develop a significant amount of biomass.

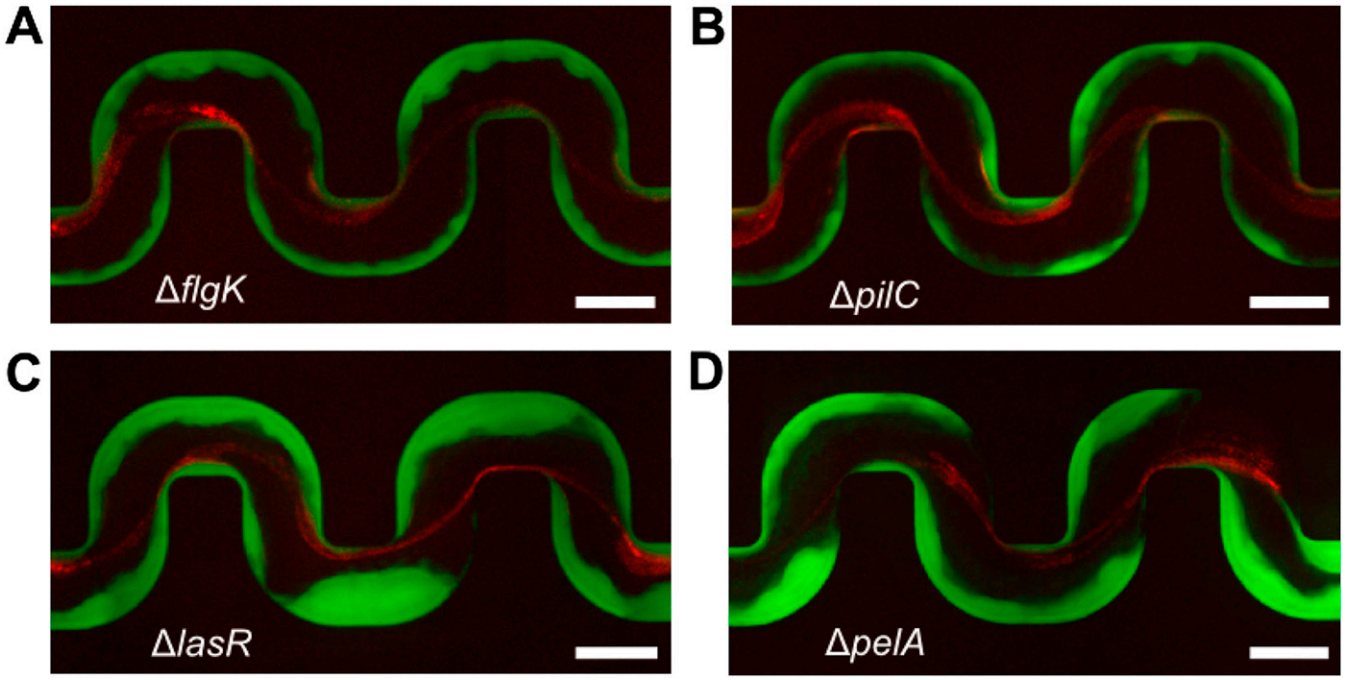

Fig. S7. Mutants get caught in wild-type EPS. For the first 43 h, PA14-*gfp* is flowed through the channel, and cells build a wall-attached biofilm. The in-flowing culture is then exchanged to only contain cells expressing *mCherry*. The GFP and mCherry color intensity is scaled between the minimum and maximum pixel intensity in each channel. (*A*) The Δ*flgK mCherry* strain forms streamers after 5 h. (*B*) The Δ*pilC mCherry* strain forms streamers after 7 h. (*C*) The Δ*lasR mCherry* strain forms streamers after 16 h. (*D*) A part of the PA14-*gfp* biofilm detached from the wall at 17.5 h and triggered streamer formation of the Δ*pelA mCherry* strain. Scale bar: 200 μm.

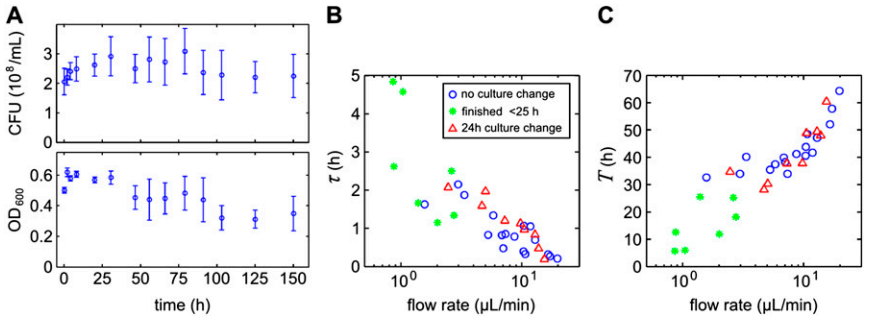

Fig. S8. Changes in the reservoir culture. (*A*) We simultaneously monitored the OD_{600} and CFU concentration of *P. aeruginosa* wild-type cultures in $n = 6$ independent reservoirs over time. Both measurements remain roughly constant for ∼3 d. (*B*, *C*) The clogging duration τ and time of clogging T are similar for experiments in which the culture in the reservoir is exchanged every 24 h, compared with experiments in which the culture is not exchanged.

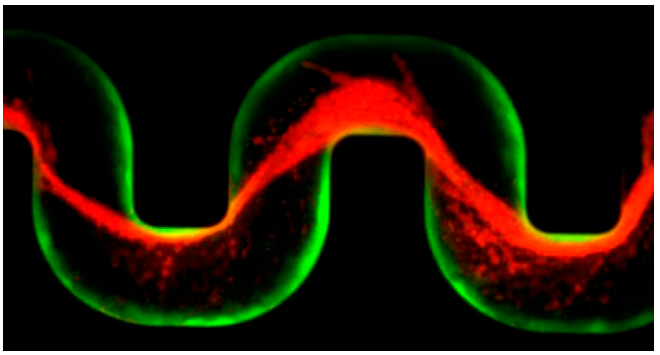

Movie S1. Flow brings bacteria to the clogging site. For the first 43 h, *P. aeruginosa* expressing *gfp* are flown through the channel. The in-flowing culture is then exchanged to contain only cells that make the red fluorescent protein mCherry, but are otherwise isogenic. This movie illustrates that the wall-attached biofilm is made up of green cells, whereas the streamer is made up exclusively of red cells, which were transported to the clogging site by flow.

Movie S1

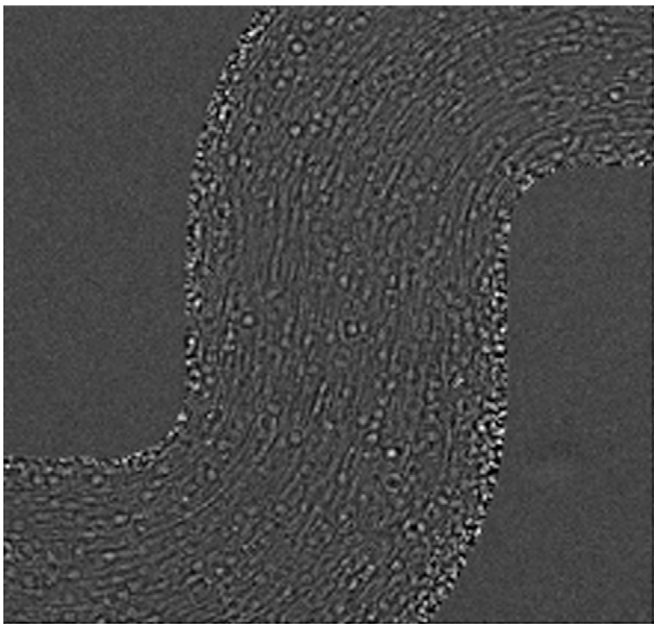

Movie S2. Biofilm streamer initiation. Several snapshots of this movie are shown in Fig. S3. This movie is displayed at 5× real time. Images were acquired using bright-field microscopy, and a background image was subtracted to visualize newly appearing structures such as streamers. The background image is made from the average of the 10 images taken 5 s before each image shown.

Movie S2